ELSEVIER

International Journal of Solids and Structures 40 (2003) 7357–7374

INTERNATIONAL JOURNAL OF SOLIDS and STRUCTURES

www.elsevier.com/locate/ijsolstr

Modeling of crack growth in ductile solids: a three-dimensional analysis

Jinkook Kim, Xiaosheng Gao *, T.S. Srivatsan

Department of Mechanical Engineering, The University of Akron, 302 Buchtel Mall, Akron, OH 44325, USA

Received 8 May 2003; received in revised form 19 August 2003

Abstract

A population of several spherical voids is included in a three-dimensional, small scale yielding model. Two distinct void growth mechanisms, put forth by [Int. J. Solids Struct. 39 (2002) 3581] for the case of a two-dimensional model containing cylindrical voids, are well contained in the model developed in this study for spherical voids. A material failure criterion, based on the occurrence of void coalescence in the unit cell model, is established. The critical ligament reduction ratio, which varies with stress triaxiality and initial porosity, is used to determine ligament failure between the crack tip and the nearest void. A comparison of crack initiation toughness of the model containing cylindrical voids with the model containing spherical voids reveals that the material having a sizeable fraction of spherical voids is tougher than the material having cylindrical voids. The proposed material failure determination method is then used to establish the fracture resistance curve (J–R curve) of the material. For a ductile material containing a small volume fraction of microscopic voids initially, the void by void growth mechanism prevails, which results in a J–R curve having steep slope. On the other hand, for a ductile material containing a large volume fraction of initial voids, the multiple voids interaction mechanism prevails, which results in a flat J–R curve. Next, the effect of T-stress on fracture resistance is examined. Finally, nucleation and growth of secondary microvoids and their effects on void coalescence are briefly discussed.

Keywords: Ductile fracture; Void growth and coalescence; Void by void growth; Multiple voids interaction; Secondary microvoids; Unit cell analysis; Fracture toughness

1. Introduction

Ductile fracture in metallic alloys usually follows a multi-step failure process involving several concurrent and mutually interactive mechanisms (Van Stone et al., 1985; Garrison and Moody, 1987). Essentially these mechanisms, at the microscopic level, include the following: (a) nucleation of microscopic voids by either fracture or decohesion of the second-phase particles and inclusions, (b) growth of the fine microscopic voids due to localized plastic deformation and eventual coalescence, (c) localization of plastic

* Corresponding author. Tel.: +1-330-972-2415; fax: +1-330-972-6027.
E-mail address: xgao@uakron.edu (X. Gao).

0020-7683/$ - see front matter © 2003 Elsevier Ltd. All rights reserved.
doi:10.1016/j.ijsolstr.2003.08.022

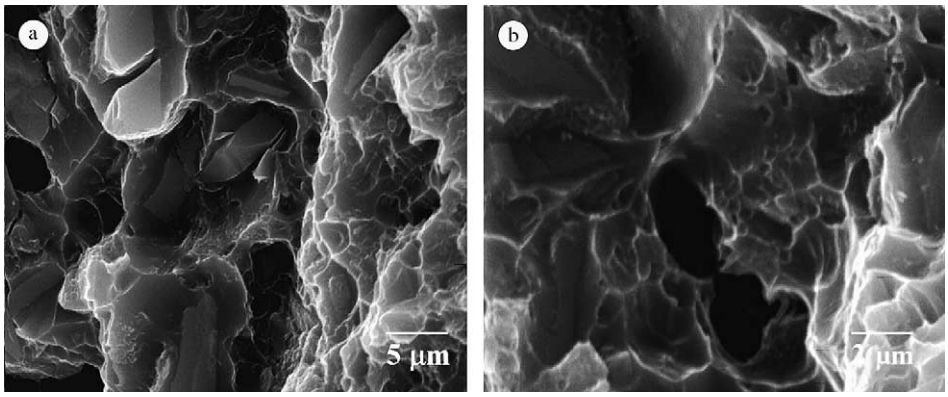

Fig. 1. SEM fractograph of ductile fracture in an aluminum alloy (AA2009) showing that the fracture surface is filled with voids of different size scales. (a) Formation of voids around cracked second phase particles. (b) Void coalescence to form microscopic crack.

flow between the growing voids, and (d) final tearing or rupture of the ligaments between the grown and enlarged voids. Fig. 1 is a SEM fractograph of ductile fracture in an aluminum alloy showing that the fracture surface is filled with voids of different size scales. Understanding the phenomenon of cracking in ductile materials under the conjoint influence of the applied load and structural geometry has necessitated the need to study the intrinsic mechanisms governing microscopic void formation, their growth and eventual coalescence by failure of the ligaments between the advancing crack tip and the voids, or between neighboring voids.

Mechanism-based fracture mechanics attempts to link micro-structural variables and continuum properties of the material to macroscopically measured fracture resistance. This provides a meaningful insight to support the development of predictive fracture models for an assessment of structural components. Two types of approach have been proposed in the published literature to implement the mechanism-based concepts. In the first approach the voids are considered to be implicit. The feature of this approach (Gurson, 1977; Tvergaard, 1982; Needleman and Tvergaard, 1987; Koplik and Needleman, 1988; Bilby et al., 1993; Brocks et al., 1995; Xia and Shih, 1995; Faleskog et al., 1998; Gao et al., 1998a,b) is that the events governing void nucleation, progressive growth and eventual coalescence are included in the numerical problem. This is achieved by using void containing elements based on the continuum damage models, e.g., the Gurson–Tvergarrd constitutive model (Gurson, 1977; Tvergaard, 1982). A distinct advantage of this approach is that either one or two elements can be used to represent the presence of a microscopic void in the material. The sizeable difference associated with characteristic length scales is reduced to a manageable problem. However, the primary disadvantage of this approach is that a precise constitutive model, which represents the behavior of a void containing material, is needed.

In the second approach the voids are considered to be explicit. In this approach, the shape of voids is modeled using refined finite elements. Due to the computational limitations, only a limited number of voids can be considered in this model. An exact implementation of void growth behavior is the distinct advantage of this approach. For void coalescence to occur, a failure criterion for the ligament between a void and the crack tip is needed in order to establish crack advance. The published literatures in this area are mainly two-dimensional. Aravas and McMeeking (1985a,b) critically examined the interaction between the crack tip and a cylindrical void under the plane strain, small scale yielding conditions. Several criteria were put forth for coalescence of the crack tip with the void and the fracture initiation toughness was estimated. Arun Roy and Narasimhan (1999) investigated the effect of crack tip constraint on void growth under mixed Modes I and II loading. Yan and Mai (1998) analyzed the growth of a single cylindrical void positioned ahead of a blunt crack tip in a specimen subjected to three-point bending. A variety of crack lengths and void volume

fractions were examined. In these studies, only a single void is presented in the crack tip region. In a subsequent study, Gu (2000) considered the presence of multiple voids ahead of a crack tip, where six cylindrical voids were inserted ahead of the crack for both the compact tension and center-cracked tension specimens. More recently, Tvergaard and Hutchinson (2002) investigated two distinct mechanisms for ductile crack initiation and growth using the plane strain, modified boundary layer (MBL) model containing multiple cylindrical voids. The two mechanisms are the void by void growth mechanism, which can be explained by interaction of a single void with the crack tip and the subsequent void by void advance of the tip and the multiple void interaction mechanism, which can be described by simultaneous interaction of multiple voids on the plane ahead of the crack tip both during initiation and subsequent crack growth. They found that the transition of two mechanisms is primary governed by the initial void volume fraction. That is, the material with smaller initial void volume fraction shows the void by void growth mechanism and the material with larger initial void volume fraction exhibits the multiple voids interaction mechanism.

There exists limited documentation in the published literature on three-dimensional analysis of materials containing spherical voids. Kuna and Sun (1996) investigated the influence of void arrangement on the macroscopic deformation and softening behavior of a unit cell and found that the three-dimensional plane strain model containing a spherical void is stiffer than the two-dimensional plane strain model having a cylindrical void. Hom and McMeeking (1989) used the three-dimensional MBL model to analyze the interaction between a growing void and the crack tip. Their results reveal that the microscopic void positioned ahead of an advancing crack grew faster towards the crack tip direction and the resultant void had an oblate shape. This convincingly reveals that the interaction between the growing void and the advancing crack tip is strong and overcomes the effect of a tensile stress field present ahead of the crack tip, which would tend to elongate the void in the tensile direction. Their study also revealed that the initially cylindrical voids grew five times faster than the rate of spherical voids. The coalescence criteria initially proposed by Rice and Johnson (1970), and subsequently by Le Roy et al. (1981) were used to determine the initiation of crack growth. The predicted fracture initiation toughness from the model containing a spherical void was higher than from the model containing a cylindrical void.

The objective of this paper is similar in approach to the research documented by Tvergaard and Hutchinson (2002) but the analysis here is three-dimensional. Several spherical voids are included in the three-dimensional MBL model to understand (a) the nature of void growth rate, (b) the critical ligament reduction ratio for ligament failure by void coalescence and (c) the macroscopic stress–strain behavior of a representative material volume containing an embedded void. A procedure to predict crack initiation is established based on the results of extensive unit cell analyses. Results of the J–R curve for early stages of crack propagation are presented and discussed. The effect of T-stress on fracture resistance is also examined. Finally, nucleation and growth of secondary microvoids and their effects on void coalescence are briefly discussed.

2. Finite element modeling

This study considers the Mode I, small scale yielding (SSY) problem, i.e., the plastic zone size is assumed to be small comparing to the geometric dimensions of the specimen. In ductile metals, voids often nucleate at relatively low stress levels due to fracture or decohesion of the large inclusions. For the purpose of analysis, voids are assumed to be present in the material at the onset of loading. Further, it is assumed that the pre-existing voids have a spherical shape and the microscopic voids are distributed periodically as shown in Fig. 2(a). In an attempt to rationalize fracture behavior, a local coordinate system is set up such that x-axis represents the crack propagation direction, y-axis represents the crack opening direction and z-axis represents the thickness direction. Considering the existence of symmetry about the crack plane, only half of the region needs to be modeled. Additionally, it is assumed that deformation along the thickness

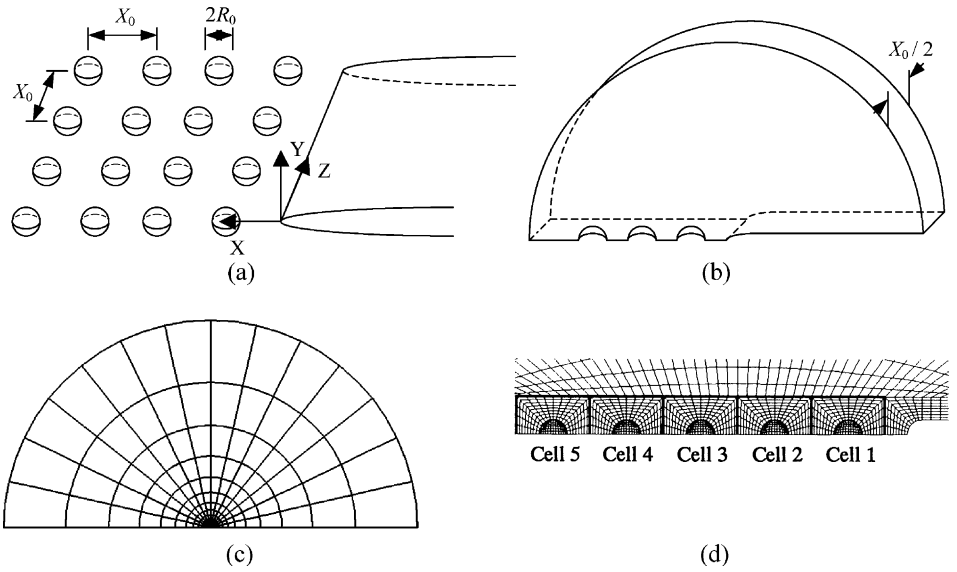

Fig. 2. (a) Periodical distribution of voids in the plane of crack propagation. (b) Domain of the boundary value problem. (c) Finite element mesh of the SSY model containing five initially spherical voids. (d) Close-up of the crack tip region showing an array of five unit cells with each cell being a cube containing a centered, spherical void.

direction of the specimen is periodically symmetric. This obviates the need to consider edge effects, which are prevalent near the surface of the specimen. Due to the periodic distribution of voids, only half of the void spacing distance is modeled through the thickness, Fig. 2(b). Both void spacing and void volume fraction can be varied by changing the ratio of X_0/R_0 where X_0 represents the initial spacing between voids situated on the crack plane or the spacing between the crack tip and the nearest void and R_0 is the initial radius of the void. Boundary conditions are prescribed on the planes normal to z-direction as

$$\begin{aligned} u_z &= 0, \\ t_x &= 0, \\ t_y &= 0, \end{aligned} \tag{1}$$

where u_z represents the displacement component in z-direction, t_x and t_y represent the components of surface traction in x- and y-directions respectively.

To resolve the crack tip deformation field and enhance convergence of the nonlinear iterations, the finite element mesh contains an initial root radius at the crack tip. Previous studies have shown that the influence of initial root radius becomes negligible if it is sufficiently small comparing to the void spacing. Here the initial root radius of the crack tip is taken to be the same as the initial radius of the void. Numerical solutions are generated by imposing displacements of the elastic, asymptotic Mode I field (plane strain) on the outer circular boundary. In this study, the radius of the outer circular boundary is taken to be 10,000 times the initial void spacing to assure the small scale yielding conditions being satisfied. The displacements at the outer boundary are given by

$$\begin{aligned} u_x &= \frac{1+v}{E}\sqrt{\frac{r_0}{2\pi}}\left\{K_{\mathrm{I}}\cos\frac{\theta}{2}\left(2-4v+2\sin^2\frac{\theta}{2}\right)\right\}+\frac{(1-v^2)}{E}Tr_0\cos\theta, \\ u_y &= \frac{1+v}{E}\sqrt{\frac{r_0}{2\pi}}\left\{K_{\mathrm{I}}\cos\frac{\theta}{2}\left(4-4v-2\cos^2\frac{\theta}{2}\right)\right\}-\frac{v(1+v)}{E}Tr_0\sin\theta, \end{aligned} \tag{2}$$

where K_I represents the Mode I stress intensity factor, T represents the nonsingular T-stress parallel to the crack plane, (r, θ) denote the crack tip polar coordinates, and r_0 is the radius of the outer circular boundary of the SSY model. Loading of the SSY model proceeds by imposing the displacement increments on the outer boundary according to the asymptotic fields. For problems having nonzero T-stress (magnitude less than yield stress), the displacements due to T-stress are imposed first. Subsequent load steps impose displacement increments corresponding to specified ΔK_I values.

Fig. 2(c) shows a typical finite element mesh of the SSY model containing five spherical voids. The mesh consists of 8184 twenty-node, isoparametric, brick elements with reduced integration. Fig. 2(d) shows a close-up of the crack tip region. It is natural to consider the material ahead of the crack tip as an array of unit cells with each cell being a cube containing a centered, spherical void, Fig. 2(d). A quarter of each cell has 96 elements around the void and eight elements in the radial direction.

The material chosen for this study obeys the power-law hardening (true) stress–strain relation

$$\begin{aligned} \varepsilon &= \frac{\sigma}{E}, \quad \sigma \leqslant \sigma_0, \\ \varepsilon &= \frac{\sigma_0}{E}\left(\frac{\sigma}{\sigma_0}\right)^{1/N}, \quad \sigma > \sigma_0, \end{aligned} \tag{3}$$

where $E = 200$ GPa, $\sigma_0 = 600$ MPa, $v = 0.3$ and $N = 0.1$, which is representative of structural steel having an intermediate strength and moderate strain hardening. The stress–strain relation is implemented in ABAQUS (2001) by using the UHARD user subroutine.

3. Results and discussions

3.1. Void by void growth versus multiple voids interaction

Performing two-dimensional plane strain analyses and assuming the presence of cylindrical voids embedded along the thickness direction, Tvergaard and Hutchinson (2002) found that there exist two failure mechanisms, single void growth mechanism and multiple voids growth mechanism. The single void growth mechanism is explained by the interaction of the crack tip with the nearest void and the subsequent advance of the crack tip from one void to the neighboring void. The multiple voids interaction mechanism is described by the simultaneous interaction of multiple voids positioned on a plane ahead of the crack tip both during initiation and stable crack growth. The transition between the two mechanisms is governed by the initial void volume fraction.

From our analysis of the three-dimensional model having spherical voids, we found similar results. To exemplify the mechanisms, we considered models having voids of varying initial volume fraction. The deformed void shapes for an initial void volume fraction of 0.0013 at the applied load level of $J/(X_0\sigma_0) = 2.73$ is shown in Fig. 3(a) and for an initial void volume fraction of 0.014 at the applied load level of $J/(X_0\sigma_0) = 0.98$ is shown in Fig. 3(b). Here J is Rice's J-integral (Rice, 1968) and $J = (1 - v^2)K_I^2/E$ for small scale yielding and plane strain conditions. The initial void volume fraction is given by $f_0 = 4\pi R_0^3/(3X_0^3)$. In Fig. 3(a), only the first void from the crack tip has significant volume increase while in Fig. 3(b), the volume of several voids increases simultaneously. Fig. 4(a) and (b) compare the void growth rates in four unit cells ahead of the crack tip for the $f_0 = 0.0013$ case and the $f_0 = 0.014$ case respectively. A conclusion can be drawn from the results shown in Figs. 3 and 4. For the case of a material having low initial void volume fraction, only the void nearest to the crack tip undergoes a significant amount of growth. This rationalizes well the single void growth mechanism. In contrast, for a material having large initial void volume fraction, several of the microscopic voids positioned directly ahead of the crack tip grow

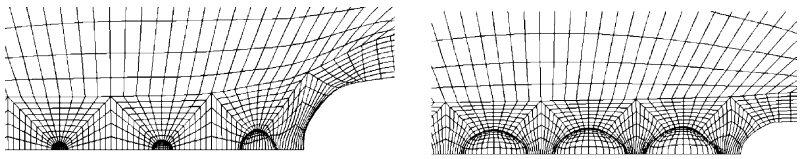

(a) (b)

Fig. 3. Deformed finite element meshes showing two distinct void growth mechanisms. (a) $f_0 = 0.0013$ and $J/(X_0/\sigma_0) = 2.73$, (b) $f_0 = 0.014$ and $J/(X_0/\sigma_0) = 0.98$.

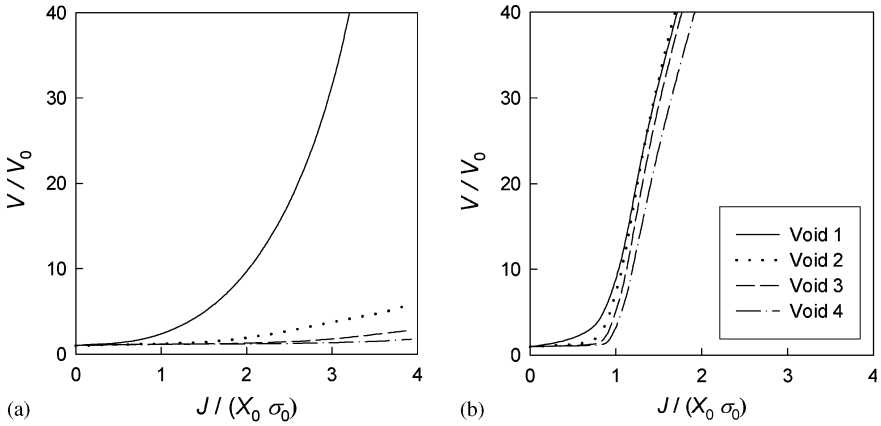

Fig. 4. Comparison of the void growth rates in four unit cells ahead of the crack tip for (a) the $f_0 = 0.0013$ case and (b) the $f_0 = 0.014$ case respectively showing the void by void growth mechanism and the multiple void interaction mechanism.

concurrently. This rationalizes well the multiple voids interaction mechanism. Consequently, fracture toughness will decrease as the increase of the initial void volume fraction.

To demonstrate the occurrence of interactions between neighboring voids for the multiple void growth mechanism, the model containing five voids is compared with a model containing only one void. Fig. 5 shows the deformed void shape for the single void model. The deformed void shapes for $f_0 = 0.0013$ and $J/(X_0\sigma_0) = 2.73$ is shown in Fig. 5(a) and for $f_0 = 0.014$ and $J/(X_0\sigma_0) = 0.98$ is shown in Fig. 5(b). Comparing with Fig. 3(a) and (b), the deformed shape of the model based on a single void is quite similar to the deformed shape of the model containing five voids for the case of small initial void volume fraction ($f_0 = 0.0013$). However, the deformed shapes are drastically different the case of large initial void volume fraction ($f_0 = 0.014$). Fig. 6(a) compares the growth rate of the nearest void from crack tip between the

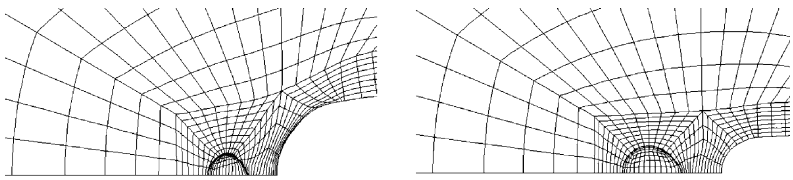

(a) (b)

Fig. 5. Deformed meshes of the SSY model containing only one void. (a) $f_0 = 0.0013$ and $J/(X_0\sigma_0) = 2.73$, (b) $f_0 = 0.014$ and $J/(X_0\sigma_0) = 0.98$.

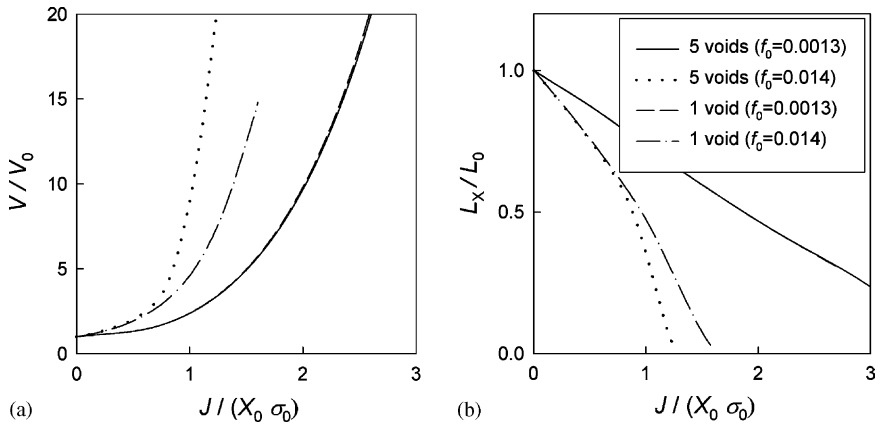

Fig. 6. Comparison of the predicted (a) growth rate of the first void from the crack tip and (b) size reduction ratio of the first ligament obtained using the single void model and the model containing five voids.

single void model and the model containing five voids and Fig. 6(b) compares the reduction of the ligament between the advancing crack tip and the nearest void between the two models. The comparison are made for two initial void volume fractions, $f_0 = 0.0013$ and $f_0 = 0.014$. For the case of low initial porosity, the two models do not reveal any noticeable difference in void growth rate and the reduction rate of the ligament between the crack tip and the nearest void. However, there is a noticeable difference for the case of high initial porosity. These observations help us conclude that interaction exists between neighboring voids for the case of large initial void volume fraction and the model containing one single void is not adequate to predict the fracture toughness of the material.

3.2. Macroscopic behavior of a representative material volume

Assuming the existence of a periodic distribution of voids, the material can be considered as an array of cubic blocks with each block being a unit cell having a void at its center. The macroscopic stress–strain behavior of the unit cell is very important in developing the void containing element based on the continuum damage models or to aid in calibrating the parameters in the constitutive model (Kim et al., 2003). Analyzing the process of void growth and coalescence in the unit cell is also necessary for establishment of the ligament failure criterion.

The macroscopic stresses and strains of cells in the SSY model are computed as follows

$$\begin{aligned} \Sigma_{ij} &= \frac{1}{V}\int_V \sigma_{ij}\,\mathrm{d}V, \\ E_{ij} &= \sum \Delta E_{ij}, \end{aligned} \tag{4}$$

where $\Delta E_{ij} = \frac{1}{2V}\int_S(\Delta u_i n_j + \Delta u_j n_i)\,\mathrm{d}S$ and $V = \int_S x_1 n_1\,\mathrm{d}S$. In above equations, Σ_{ij} represent the macroscopic stress components, σ_{ij} represent the (true) stress components of the matrix, V is the volume of the cell including the void, E_{ij} represent the macroscopic strain components, u_i denote the nodal displacement components, and S is the outside surface of the cell with n_i being the components of the normal vector of S. These values are evaluated using the finite element integration scheme (Zienkiewicz, 1977). The macroscopic effective stress (Σ_e), hydrostatic stress (Σ_h) and effective strain (E_e) are given by

$$\Sigma_e = \frac{1}{\sqrt{2}}\left[\left(\Sigma_{xx}-\Sigma_{yy}\right)^2+\left(\Sigma_{yy}-\Sigma_{zz}\right)^2+\left(\Sigma_{zz}-\Sigma_{xx}\right)^2\right]^{1/2},$$
$$\Sigma_h = \frac{1}{3}(\Sigma_{xx}+\Sigma_{yy}+\Sigma_{zz}), \tag{5}$$
$$E_e = \frac{\sqrt{2}}{3}\left[(E_{xx}-E_{yy})^2+(E_{yy}-E_{zz})^2+(E_{zz}-E_{xx})^2\right]^{1/2}.$$

To characterize the macroscopic stress state of the cell, the following stress ratios are introduced

$$T = \frac{\Sigma_h}{\Sigma_e}, \quad \rho_1 = \frac{\Sigma_{xx}}{\Sigma_{yy}}, \quad \rho_2 = \frac{\Sigma_{zz}}{\Sigma_{yy}}. \tag{6}$$

Zhang et al. (2001) and Kim et al. (2003) studied the effects of the triaxial stress state and found that the stress triaxiality ratio T alone cannot uniquely characterize the effect of macroscopic stress state on void growth and coalescence. The Lode parameter should be used to distinguish different stress states having the same stress triaxiality ratio. Defining

$$\tan\theta = \frac{2\Sigma_{zz}-\Sigma_{yy}-\Sigma_{xx}}{\sqrt{3}(\Sigma_{yy}-\Sigma_{xx})}, \tag{7}$$

Zhang et al. (2001) and Kim et al. (2003) showed that a cell when subject to the same stress triaxiality ratio would tend to react differently when θ is different. The stress triaxiality ratio along with the parameter θ can be used to specify stress state.

Fig. 7 shows the variation of Σ_e, T, ρ_1 and θ as the increase of applied load J for four cells ahead of the crack tip. Here the initial void volume fraction is $f_0 = 0.0079$. As expected, the stress triaxiality ratio T and the parameter θ are not constant during the loading history. The triaxiality ratio increases with applied J in the plastic deformation region of the cell. A sudden increase in triaxiality ratio occurs due essentially to collapse of the cell and rapid drop of Σ_e. The parameter θ also increases with the applied load. This is because the stress ratio in the thickness direction becomes larger as the applied J increases. Interestingly, except for cell 1, the stress ratio ρ_1 remains almost a constant during the loading history. The deviation of ρ_1 for cell 1 can be explained by the constraint loss of the crack tip due to blunting.

Fig. 8 compares the evolution of the macroscopic effective stress and the stress triaxiality ratio of cell 1 for different initial void volume fractions, $f_0 = 0.0013$, 0.0035, 0.0079 and 0.014. Initially, the effective macroscopic stress increases with the applied J. Upon reaching the peak stress, the effective macroscopic stress decreases rationalizing the occurrence of softening due to void growth, Fig. 8(a). The peak stress value decreases and the J value for onset of coalescence reduces as f_0 increases. The stress triaxiality ratio of cell 1 decreases during macroscopic elastic deformation of the cell. Depending on the level of initial porosity the triaxiality ratio either increases, or conversely increases and then decreases in the plastic range, Fig. 8(b). The stress triaxiality ratio is lower for the cell having smaller f_0 value.

3.3. Crack initiation

Macroscopic crack initiation is said to have occurred upon coalescence of the growing voids with the crack tip. Several mechanistic observations have been put forth to explain void coalescence. Coalescence can occur either through shear band formation or through formation of "void sheets", i.e., nucleation and growth of secondary and smaller voids in the ligament between larger voids. In some cases, the voids grow till they impinge with the other voids or crack tip.

It is difficult to implement these coalescence mechanisms directly to the numerical model. As a viable alternative several criteria based on the length of the ligament relative to the size of the void have been proposed. Rice and Johnson (1970) suggested coalescence to occur when

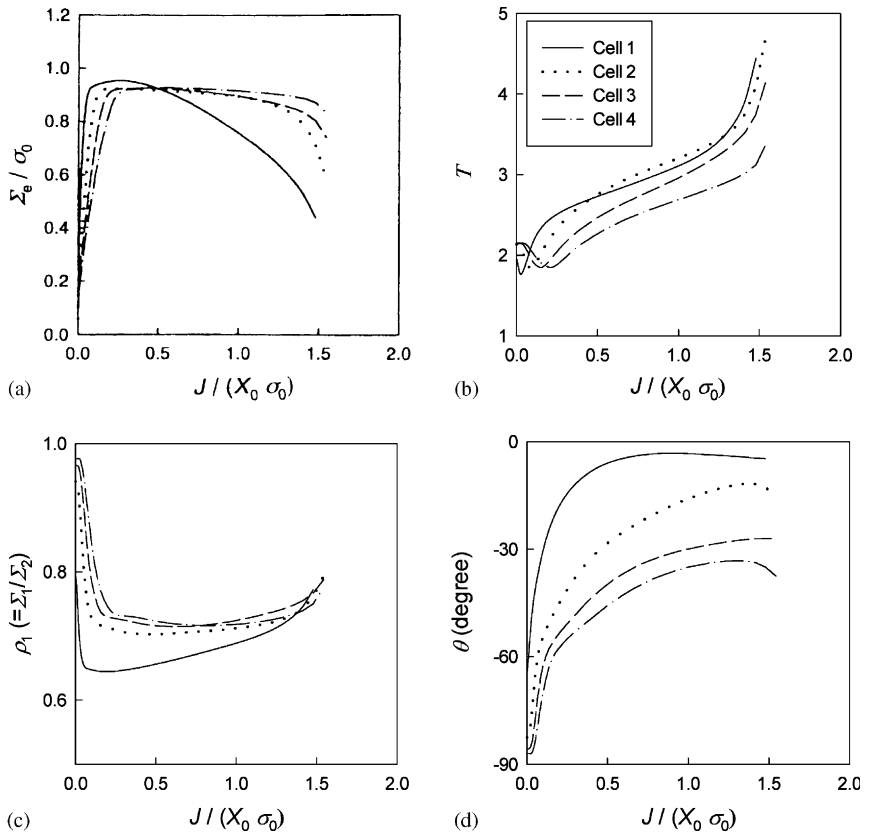

Fig. 7. Variation of (a) the macroscopic effective stress Σ_e, (b) the stress triaxiality ratio T, (c) the macroscopic stress ratio ρ_1 and (d) the parameter θ with the applied load J for the four cells, where cell 1 is the first from the crack tip and J represents the J-integral.

$$\gamma = \frac{L_x}{V_y} \tag{8}$$

reaches a critical value, such as one, where L_x is the length of the deformed ligament between the void and crack tip, and V_y is dimension of the void in the crack opening direction. Brown and Embury (1973) proposed void coalescence to occur through the conjoint influences of shear band development and void impingement when the ratio of ligament length to the void dimension reached a critical value. In a companion study, Le Roy et al. (1981) proposed an empirical relationship for void coalescence to occur only when

$$\phi = \frac{2R_3^f}{L_x} \tag{9}$$

reaches a critical value, where $2R_3^f$ is dimension of the void along the longest axis (major axis). Based on experimental data the value of ϕ was suggested as 0.83 for the case of spherical voids. In their recent paper, Tvergaard and Hutchinson (2002) used the ligament reduction ratio

$$\chi = \frac{L_x}{L_0} \tag{10}$$

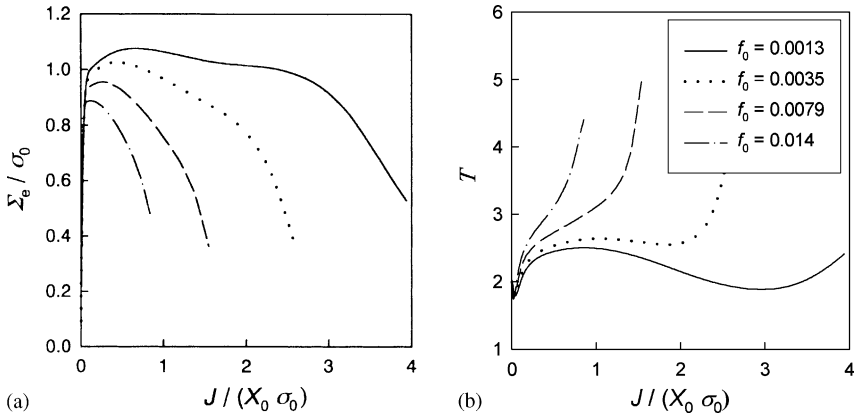

Fig. 8. Variation of (a) the macroscopic effective stress and (b) the stress triaxiality ratio of cell 1 during the loading history for different initial void volume fractions, $f_0 = 0.0013$, 0.0035, 0.0079 and 0.014.

as the parameter for the failure criterion. Here L_0 is the size of the initial ligament between the growing void and the advancing crack tip and L_x is the size of the deformed ligament. In their study, a critical ligament reduction ratio (χ_c) of either 1/2 or 1/3 was used.

Our recent studies suggest that the ligament reduction ratio at the onset of coalescence is not a constant. The critical ligament reduction ratio depends on the initial void volume fraction and the stress state in the ligament. Considering the material composed of void containing cells, failure of the ligament between neighboring voids corresponds to process of internal necking. To determine the critical ligament reduction ratio for void coalescence, consider a unit cell containing a centered, spherical void. Coalescence (internal necking) will occur when the macroscopic deformation of the cell shifts to a uniaxial strain state (Koplik and Needleman, 1988). To utilize this idea, we analyze a cubic cell having a spherical void at its center and subjected to loading conditions similar to the cells in the SSY models discussed in the previous section. A one-eighth symmetric finite element mesh of the unit cell model and the resultant deformed shape are shown in Fig. 9. Displacement boundary conditions are prescribed on the outer surfaces of the cell. The displacement component in z-direction is constrained on the face normal to z-axis. The displacement components are specified on the faces perpendicular to x-axis and y-axis incrementally using the procedure developed by Faleskog et al. (1998) so that the macroscopic stress ratio $\rho_1 = \Sigma_{xx}/\Sigma_{yy}$ remain constant

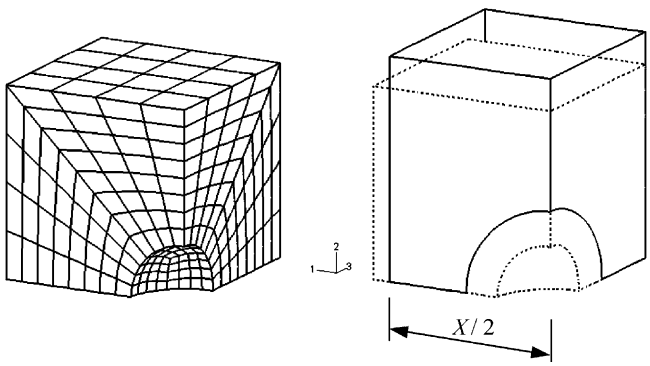

Fig. 9. A one-eighth symmetric finite element mesh and the deformed shape for the unit cell containing a centered, spherical void.

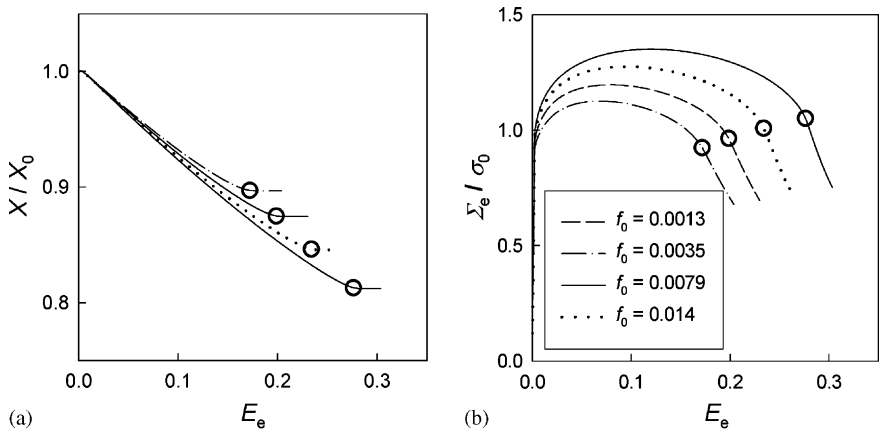

Fig. 10. (a) Variation of the deformed cell width in x-direction with the macroscopic effective strain of the cell revealing the shift to uniaxial straining. (b) Macroscopic effective stress versus effective strain of the cell displaying the macroscopic softening. Here ρ_1 is specified as 0.54 and the symbols denote the onset of coalescence.

during the loading history. Variation of the deformed cell width in x-direction with the macroscopic effective strain of the cell, shown in Fig. 10(a), reveals the shift to uniaxial straining. Fig. 10(b) shows the macroscopic effective stress versus effective strain for the cell displaying the macroscopic softening. The cubic unit cells were analyzed for various void volume fractions (f_0) and for a fixed stress ratio of $\rho_1 = 0.54$. The variation of macroscopic effective stress is shown in Fig. 10(b). The circles in Fig. 10 represent the onset of uniaxial straining mode, i.e., void coalescence.

The unit cell analyses were conducted for varying initial void volume fraction, $f_0 = 0.0009, 0.0013, 0.002, 0.0035, 0.0079, 0.014$ and 0.02182 and several values of stress ratio, $\rho_1 = 0.44, 0.54, 0.64$ and 0.74. Both the ligament reduction ratio (χ) and the ratio of ligament size to void size along the crack opening direction (γ) were calculated at the onset of void coalescence. Fig. 11(a) reveals the variation of critical ligament reduction ratio (χ_c) as a function of ρ_1 and f_0 while Fig. 11(b) shows the critical ratio of ligament size to void size in the crack opening direction (γ_c) as a function of ρ_1 and f_0. Both χ_c and γ_c are not constant but

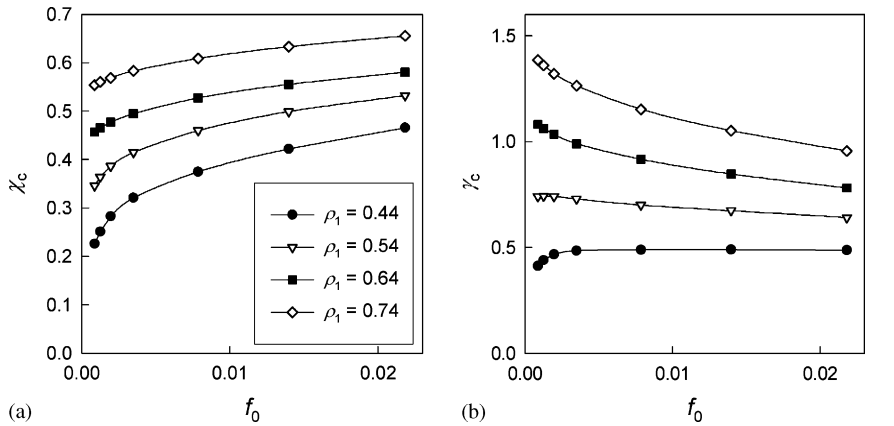

Fig. 11. (a) Variation of the critical ligament reduction ratio (χ_c) as a function of ρ_1 and f_0. (b) Variation of the critical ratio of ligament size to void size in the crack opening direction (γ_c) as a function of ρ_1 and f_0.

functions of the stress state and initial void volume fraction. An increase in either initial void volume fraction or applied stress ratio tends to increase χ_c.

To apply these results in the SSY model to predict crack initiation, it is necessary to estimate the macroscopic stress ratio ρ_1 of the ligament between the crack tip and the first void. However, it is difficult to calculate the ligament stress ratio ρ_1 directly. We approximate the ligament ρ_1 value by extrapolation. In Fig. 3(b), it is visualized that cell 1 is positioned at a distance of $0.5X_0$ and cell 2 has a distance of $1.5X_0$ from the first ligament. Therefore, ρ_1 of the first ligament can be extrapolated using the macroscopic stress ratios calculated for cell 1 and cell 2. By comparing the extrapolated ρ_1 value for the first ligament of SSY model to ρ_1 values and critical ligament reduction ratios (χ_c) of the unit cell for a given initial void volume fraction, it is possible to determine the applied J at which the first void coalesce with the crack tip. This applied J value can be regarded as the fracture initiation toughness (J_{Ic}).

Using the above approach, the variation of J_{Ic} with f_0 can be predicted. Fig. 12 shows the dependence of J_{Ic} on the initial void volume fraction. The value of J_{Ic} increases with decreasing f_0. For small values of f_0 where material failure occurs as a consequence of void by void growth, the material exhibits large resistance to fracture initiation. Fracture toughness can be improved significantly by reducing the initial porosity. As f_0 increases, fracture toughness decreases. At some level of f_0 a transition of failure mechanism to the multiple voids interaction occurs.

Fig. 12 also compares the predicted fracture initiation toughness in this study with he results obtained using the constant critical ligament ratio of 1/2 for the three-dimensional model with spherical voids. It can be seen that using $\chi_c = 1/2$ the fracture toughness is over-predicted for large values of f_0 but under-predicted for small values of f_0.

For comparison, the two-dimensional results by Tvergaard and Hutchinson (2002) obtained using a constant critical ligament reduction ratio of 0.5 for the cylindrical voids are also displayed in Fig. 12. It can be seen that the three-dimensional model with spherical voids predicts higher fracture toughness than the two-dimensional model with cylindrical voids. At high values of initial void volume fraction ($f_0 > 0.02$), both models reveal marginal difference in fracture toughness. However, the discrepancy in fracture toughness of the two models becomes prominent for low values of initial void volume fraction. For a void volume fraction of 0.0013 the material containing spherical voids is 1.6 times tougher (in terms of J_{Ic}) than the material containing cylindrical voids.

Fig. 13 shows the comparison of the estimated toughness to the experimentally measured data summarized in McMeeking (1977) and Tvergaard and Hutchinson (2002). The experimental data are repre-

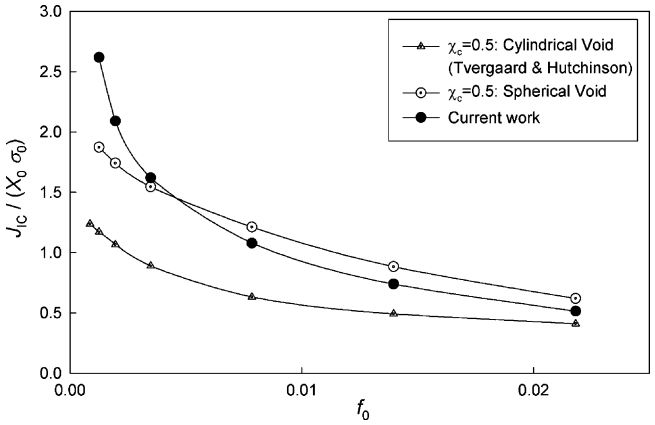

Fig. 12. Variation of normalized fracture initiation toughness (J_{Ic}) with initial void volume fraction (f_0) predicted using different material failure criteria.

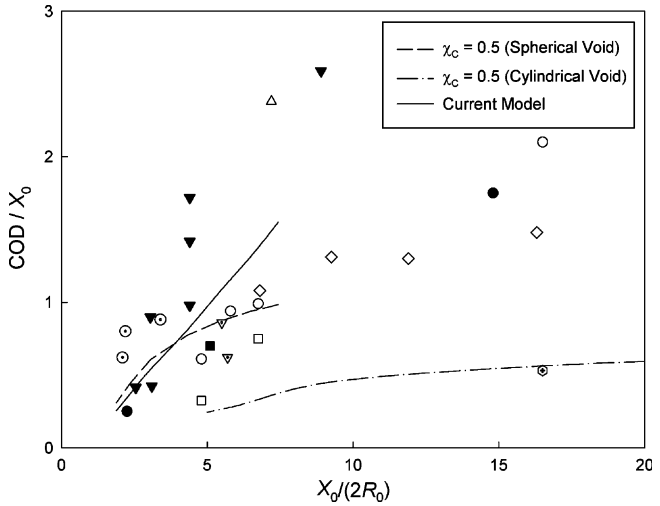

Fig. 13. Comparison of the estimated fracture initiation toughness to the experimentally measured data summarized in McMeeking (1977) and Tvergaard and Hutchinson (2002). The experimental data are represented by symbols.

sented by symbols and pretty much scattered. It is important to note that the experiments were conducted for several materials and the material properties are not same. Since the vertical axis of the original graph is COD normalized by void spacing, a relation $\mathrm{COD} = 0.5J_{\mathrm{Ic}}/\sigma_0$ is used to convert the computed J_{Ic} to COD as suggested by Tvergaard and Hutchinson (2002). The horizontal axis of Fig. 13 is void spacing normalized by the initial void diameter. Note that a cylindrical void represents much larger void volume fraction than a spherical void having the same X_0/R_0. The fracture toughness predicted using the two-dimensional model (cylindrical void) substantially underestimates the experimental data. Adoption of the three-dimensional model (spherical void) and a constant critical ligament reduction ratio $\chi_c = 1/2$ for ligament failure gives reasonably well estimate of J_{Ic} for materials containing high initial porosities. But for the low porosity material, the fracture toughness is underestimated. The method suggested in this study improves the prediction of fracture initiation toughness.

3.4. Crack advance

To model crack growth, the ligament nodes on the symmetry plane are released when the ligament reduction ratio reaches the critical value χ_c depending on the macroscopic stress ratio ρ_1 of the ligament and the initial porosity f_0. A sudden release of the reaction forces at the ligament nodes causes numerical instability and therefore, several increments are needed to step down the reaction forces to zero. The deformed mesh immediately following the release of the nodal reaction forces of the first ligament is shown in Fig. 14(a). Since the reaction forces, which ensure plastic deformation of the ligament, are removed, a large portion of the released ligament experiences elastic unloading with only the weakest region undergoing severe deformation. As the applied load (J) increases, the next ligament reaches the critical reduction ratio and the ligament nodes on the symmetry plane are released. The deformed mesh prior to release of the second ligament is shown in Fig. 14(b). The process continues and the crack front moves forward.

The crack growth resistance curve can be obtained by plotting the value of J at which each ligament reaches the failure criterion versus the amount of crack length increase. Crack advance takes place in discrete increments of void spacing X_0. Fig. 15 shows the fracture resistance curves for three values of initial void volume fraction, where the amount of crack growth (Δa) is normalized by X_0 and the value of J is

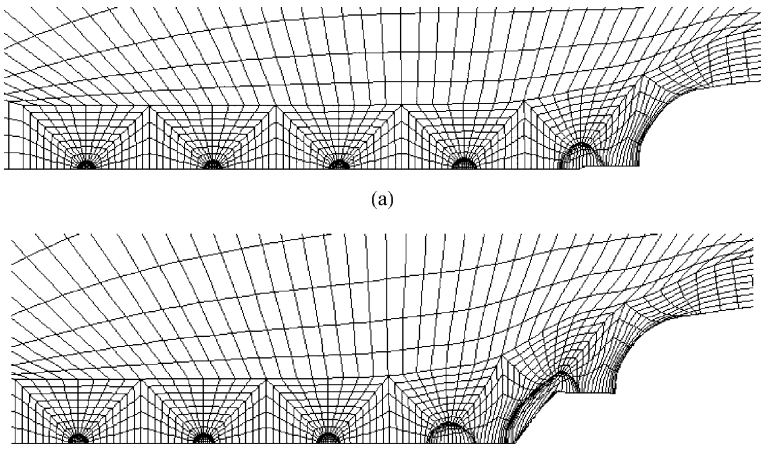

(a)

(b)

Fig. 14. Crack growth by releasing ligament nodes. (a) Deformed mesh immediately following the release of the nodal reaction forces of the first ligament. (b) Deformed mesh immediately prior to release of the second ligament.

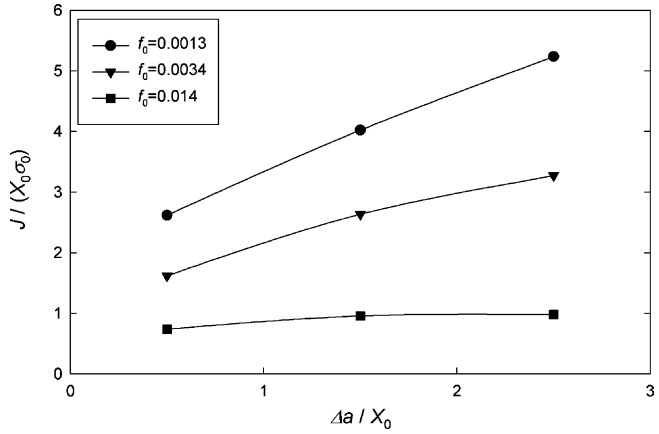

Fig. 15. Predicted fracture resistance curves for three values of initial void volume fraction, where the amount of crack growth (Δa) is normalized by X_0 and the value of J is normalized by $X_0\sigma_0$.

normalized by $X_0\sigma_0$. The fracture resistance curve for the case of large initial void volume fraction displays relatively flat slope due to the multiple voids interaction mechanism. On the other hand, for the material having small initial void volume fraction, the fracture resistance curve shows a large increase in J required to propagate the crack as a result of void by void growth mechanism.

3.5. Discussion

In the above crack initiation and growth analyses, the boundary conditions of the SSY model are prescribed according to the asymptotic K_I field and the T-stress is taken to be zero. Nonzero T-stress values can be used to study the constraint effect on ductile crack growth. Using the procedures laid out in Sections 3.3 and 3.4, there is no technical difficulty to model crack growth with nonzero T-stress. Fig. 16 shows the

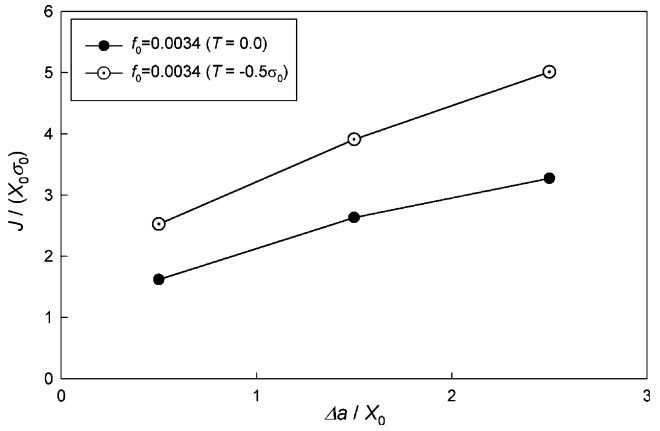

Fig. 16. Effect of negative T-stress on the fracture resistance curve.

effect of T-stress on the fracture resistance curve. As expected, negative T-stress raises the fracture resistance as well as the tearing modulus (slope of the curve).

Most engineering materials contain more than one populations of inclusions and/or second phase particles. Voids often nucleate at relatively low stress levels due to fracture or decohesion of the large inclusions. As deformation increases, large plastic flow is localized between the enlarged voids and between the void and the crack tip. Consequently, small particles in the ligaments will nucleate secondary microvoids. Rapid growth and coalescence of secondary voids will accelerate the ligament failure process. However, nucleation and growth of secondary microvoids are not taken into account in the above analyses and discussions. Therefore, the critical ligament reduction ratios determined in Section 3.3 can be regarded as lower bound values and the fracture toughness values predicted using those critical ligament reduction ratios are upper bound values for the material.

To illustrate the effects of secondary voids, we assume nucleation of the secondary voids is plastic strain controlled and the secondary voids are smeared in the material. It is further assumed that void nucleation follows a normal distribution as suggested by Chu and Needleman (1980). The rate of increase of void volume fraction due to nucleation of secondary voids is given by

$$\dot{f}_{\text{nucleation}} = D\dot{\bar{\varepsilon}}, \tag{11}$$

where

$$D = \frac{f_N}{s_N\sqrt{2\pi}} \exp\left[-\frac{1}{2}\left(\frac{\bar{\varepsilon} - \varepsilon_N}{s_N}\right)^2\right] \tag{12}$$

In above equations, $\bar{\varepsilon}$ represents the matrix plastic strain and the void nucleation parameters adopted here are $f_N = 0.004$, $\epsilon_N = 0.3$ and $s_N = 0.1$.

To account for the growth of secondary voids and its effect on material failure, the Gurson–Tvergaard constitutive model is used to describe the material behavior, i.e.,

$$\Phi = \frac{\Sigma_e^2}{\bar{\sigma}^2} + 2q_1 f \cosh\left(q_2 \frac{3\Sigma_h}{2\bar{\sigma}}\right) - 1 - q_1^2 f^2 = 0, \tag{13}$$

where the parameters q_1 and q_2 were introduced by Tvergaard (1982) to improve predictions of the original Gurson model (1977). Here $q_1 = 1.5$ and $q_2 = 1$ are used in the analysis.

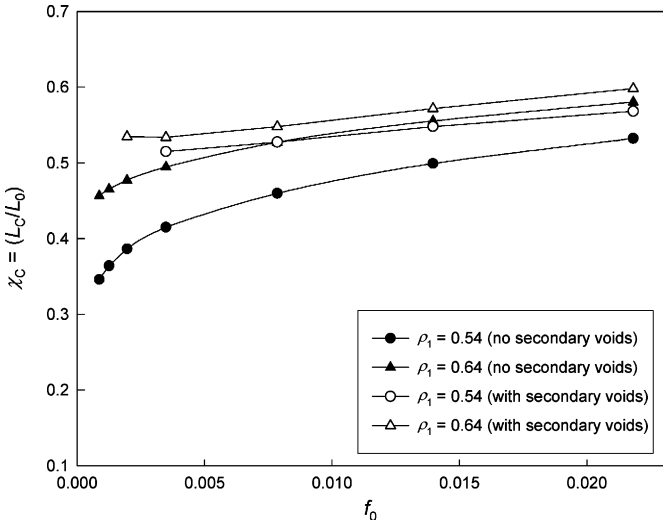

Fig. 17. Comparison of the predicted the critical ligament reduction ratios with and without secondary voids.

Now reconsider the unit cell shown in Fig. 9. Following the same procedure as outlined in Section 3.3, effects of secondary voids on the critical ligament reduction ratio can be studied. Fig. 17 compares the critical ligament reduction ratios with and without secondary voids. It is clear that nucleation and growth of secondary voids raise the critical ligament reduction ratio for coalescence, i.e., ligament failure occurs earlier with the secondary voids.

It is important to point out that the above computed χ_c values with secondary voids being considered are just for the purpose of illustrating the trends of the secondary void effect. Because the equations and parameters used to describe nucleation and growth of secondary voids are ad hoc. More detailed analyses are needed to quantify the effect of secondary voids.

4. Concluding remarks

In this study, several spherical voids are included in the three-dimensional, small scale yielding model to simulate the material failure process and ductile crack growth. Two distinct void growth mechanisms, void by void growth mechanism and multiple void interaction mechanism, initially put forth by Tvergaard and Hutchinson (2002) for the case of a two-dimensional model containing cylindrical voids, are well contained in the model developed in this study and containing spherical voids. For materials containing large initial porosity, multiple voids grow simultaneously and the interaction between voids is significant. Therefore, the model containing one single void is not adequate to predict the fracture toughness of the material.

A material failure criterion, based on the occurrence of void coalescence (internal necking) in the unit cell model, is established. The critical ligament reduction ratio, which varies with the macroscopic stress state and the initial porosity, is used to determine ligament failure between the crack tip and the nearest void. A comparison of crack initiation toughness of the model containing cylindrical voids with the model containing spherical voids reveals that the material having the same volume fraction of spherical voids is tougher than the material having cylindrical voids. The proposed material failure determination method is then used to establish the fracture resistance curve (J–R curve) of the material. For a ductile material containing a small volume fraction of microscopic voids initially, the void by void growth mechanism

prevails, which results in a J–R curve having steep slope. On the other hand, for a ductile material containing a large volume fraction of initial voids, the multiple voids interaction mechanism prevails, which results in a flat J–R curve. Numerical analyses were also performed to examine the effect of T-stress on the fracture resistance. As expected, negative T-stress raises the fracture resistance as well as the tearing modulus (slope of the curve).

The critical ligament reduction ratios computed in Section 3.3 can be regarded as lower bound values because effects of nucleation and growth of secondary microvoids are not taken into account. As a result, the fracture toughness values predicted using these critical ligament reduction ratios are upper bound values for the material. A preliminary study of the effect of secondary voids reveals that nucleation and growth of secondary voids raise the critical ligament reduction ratio for coalescence, i.e., ligament failure occurs earlier with the presence of secondary voids.

Acknowledgements

This research was made possible through research funding provided by the Office of Naval Research (N00014-02-1-0423) and by the University of Akron Faculty Research Grant.

References

ABAQUS, Standard User's Manual, Version 6.2, 2001. Hibbit, Karlsson and Sorensen Inc.

Arun Roy, Y., Narasimhan, R., 1999. A finite element investigation of the effect of crack tip constraint on hole growth under mode I and mixed mode loading. Int. J. Solids Struct. 36, 1427–1447.

Aravas, N., McMeeking, R.M., 1985a. Finite element analysis of void growth near a blunting crack tip. J. Mech. Phys. Solids 33, 25–49.

Aravas, N., McMeeking, R.M., 1985b. Microvoid growth and failure in the ligament between a hole and blunt crack tip. Finite element analysis of void growth near a blunting crack tip. Int. J. Fract. 29, 21–38.

Bilby, B.A., Howard, I.C., Li, Z.H., 1993. Prediction of the first spinning cylinder test using ductile damage theory. Fatig. Fract. Engng. Mater. Struct. 16, 1–20.

Brocks, W., Klingbeil, D.A., Kumecke, G., Sun, D.Z. 1995. Application of the gurson model to ductile tearing resistance. In: Kirk, M., Bakker, A. (Eds.), Constraint Effects in Fracture Theory and Applications. ASTM STP, 1244, Philadelphia, PA, pp. 232–254.

Brown, L.M., Embury, J.D., 1973. In: Proceedings of 3rd International Conference Strength of Metals and Alloys. Institute of Metals, London, p. 164.

Chu, C.C., Needleman, A., 1980. Void nucleation effects in biaxially stretched sheets. J. Engng. Mater. Tech. 102, 249–256.

Faleskog, J., Gao, X., Shih, C.F., 1998. Cell model for nonlinear fracture analysis-I. Micromechanics calibration. Int. J. Fract. 89, 355–373.

Gao, X., Faleskog, J., Shih, C.F., 1998a. Cell model for nonlinear fracture analysis-II. Fracture-Process calibration and verification. Int. J. Fract. 89, 375–398.

Gao, X., Faleskog, J., Shih, C.F., Dodds, R.H., 1998b. Ductile tearing in part-through cracks: experiments and cell-model predictions. Engng. Fract. Mech. 59, 761–777.

Garrison Jr., W.M., Moody, N.R., 1987. Ductile fracture. J. Phys. Chem. Solids 48, 1035–1074.

Gu, I., 2000. Finite element analyses of the deformation around holes near crack tip and their implications to the J-resistance curve. Fatig. Fract. Engng. Mater. Struct. 23, 943–952.

Gurson, A.L., 1977. Continuum of ductile rupture by void nucleation and growth: Part I—Yield criteria and flow rules for porous ductile media. J. Engng. Mater. Tech. 99, 2–55.

Hom, C.L., McMeeking, R.M., 1989. Void growth in elastic-plastic materials. J. Appl. Mech. 56, 309–317.

Kim, J., Gao, X., Srivatsan, T.S., 2003. Modeling of void growth in ductile solids: effects of stress triaxiality and initial porosity. Engng. Frac. Mech., in press.

Koplik, J., Needleman, A., 1988. Void growth and coalescence in porous plastic solids. Int. J. Solids Struct. 24, 835–853.

Kuna, M., Sun, D.Z., 1996. Three-dimensional cell model analyses of void growth in ductile materials. Int. J. Fract. 81, 235–258.

Le Roy, G., Embury, J.D., Edward, G., Ashby, M.F., 1981. A model of ductile fracture based on the nucleation and growth of voids. Acta Metall. 29, 1509–1522.

McMeeking, R.M., 1977. Finite deformation analysis crack-tip opening in elastic-plastic materials and implication for fracture. J. Mech. Phys. Solids 25, 357–381.

Needleman, A., Tvergaard, V., 1987. An analysis of ductile rupture modes at a crack tip. J. Mech. Phys. Solids 35, 151–183.

Rice, J.R., 1968. A path-independent integral and the approximate analysis of strain concentration by notches and cracks. J. Appl. Mech. Trans. ASME 35, 379–386.

Rice, J.R., Johnson, M.A., 1970. The role of large crack tip geometry changes in plane strain fracture. In: Kannine, M.F., Adler, W.F., Rosenfield, A.R., Jaffee, R.I. (Eds.), Inelastic Behavior of Solids. McGraw-Hill, New York, p. 641.

Tvergaard, V., 1982. On Localization in ductile materials containing spherical voids. Int. J. Fract. 18, 237–252.

Tvergaard, V., Hutchinson, J.W., 2002. Two mechanisms of ductile fracture: void by void growth verse multiple void interaction. Int. J. Solids Struct. 39, 3581–3597.

Van Stone, R.H., Cox, T.B., Low Jr., J.R., Psioda, J.A., 1985. Microstructural aspects of fracture by dimple rupture. Int. Met. Rev. 30, 157–179.

Xia, L., Shih, C.F., 1995. Ductile crack growth-I. A numerical study using computational cells with microstructurally-based length scales. J. Mech. Phys. Solids 43, 233–259.

Yan, C., Mai, U.W., 1998. Effect of constraint on void growth near a blunt crack tip. Int. J. Fract. 92, 287–304.

Zhang, K.S., Bai, J.B., Francois, D., 2001. Numerical analysis of the influence of the Lode parameter on the void growth. Int. J. Solids Struct. 38, 5847–5856.

Zienkiewicz, O.C., 1977. The Finite Element Method, third ed. McGraw-Hill, London.